SEMARAK ILMU PUBLISHING

Journal of Advanced Research in Fluid Mechanics and Thermal Sciences

Journal homepage:
https://semarakilmu.com.my/journals/index.php/fluid_mechanics_thermal_sciences/index
ISSN: 2289-7879

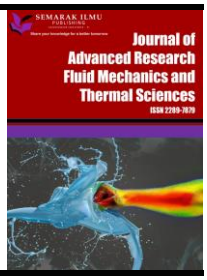


# Ship Performances CFD Analysis of Hydrofoil-Supported High-Speed Catamaran Hull Form

Ahmad Firdhaus[1], Kiryanto[1,*], Muhammad Luqman Hakim[1], Good Rindo[1], Muhammad Iqbal[1,2]

[1] Department of Naval Architecture, Faculty of Engineering, Diponegoro University, Semarang, Indonesia
[2] Department of Naval Architecture, Ocean and Marine Engineering, Henry Dyer Building, University of Strathclyde, Glasgow, Scotland, United Kingdom

**ARTICLE INFO**

***Article history:***
Received 25 September 2023
Received in revised form 15 December 2023
Accepted 28 December 2023
Available online 15 January 2024

***Keywords:***
Hydrofoil supported catamaran; high-speed catamaran; CFD; ship performance

**ABSTRACT**

Fast ferries with efficient fuel use are becoming increasingly in demand as fossil fuels become more in short supply and metropolises expand all over the globe in coastal and estuarine environments. These criteria need to be fulfilled by the Hydrofoil Supported Catamaran (HYSUCAT). A catamaran with wings between its demi hulls is known as an HYSUCAT, and it combines the positive traits of both the catamaran (manoeuvrability, big deck area) and the wing in-ground vehicle (excellent lift-to-drag ratio). In this research, a concept design Delft-372 catamaran is refitted with a high Reynolds number foil system to lower its overall resistance. The numerical solution of the Reynolds-averaged Navier–Stokes (RANS) equations employing the k-w SST turbulence model is used to simulate the flow around a high-speed catamaran with a hydrofoil. According to the simulation findings, the hydrofoil-assisted catamaran was determined to be a viable alternative to the current catamaran. This is due to a significant decrease in the overall resistance of the ship, reaching up to 42%, as well as notable improvements in pitch angle, reaching up to 26%.

## 1. Introduction

High-sped crafts are crucial in transportation and other industries. One of the most versatile high-speed crafts is multihull. Naval architects have traditionally examined these hulls for their high speed and seakeeping capabilities. Appendages have been used as energy-saving measures to minimize ship hull fuel consumption. Foils have been used to save energy in the form of Hull Vane® on single and multihull boats [1], catamarans to create hydrofoil-supported catamarans (hysucat) [2] or watercraft (hysuwac) [3], and air foil assisted catamaran (AAC) [4]. This research advances the hydrofoil-supported catamaran idea by retrofitting a foil system to a running catamaran to lower its resistance. When sailing swiftly, the lift force of the wings reduces vessel displacement and hydrodynamic resistance. Hydrofoil type and Froude number affect catamaran hydrodynamic performance.

* *Corresponding author.*
*E-mail address: kiryanto@lecturer.undip.ac.id*

https://doi.org/10.37934/arfmts.113.1.108121

Hydrodynamic performance must be predicted for various hydrofoils and Froude numbers to build an efficient hydrofoil-supported catamaran.

According to the findings of a number of investigations, research, and development of hydrofoil-supported catamarans (also known as Hysucat) and hydrofoil-supported watercraft (also known as Hysuwac) had their start at Stellenbosch University in South Africa in the late 1970s or early 1980s, when it was led by Professor Karl Gunter Hoppe [5-7]. Their research highlighted the significance of hydrofoil placement concerning a vessel's resistance, with the just-below-the-centre-of-gravity (CoG) location being deemed the most effective placement option [8]. Recent research examining the hydrodynamic performance of various hydrofoils on Hysucat catamarans was carried out by several authors and reported significant reductions in total resistance and drag, ranging from 2.14% to 50% [9-12]. These findings highlight the potential benefits of hydrofoil applications in enhancing ship efficiency.

Earlier research has shown that using hydrofoils on catamarans is very sensitive to various factors, including the configuration and kind of foil, the catamaran hull's form, and the ship's speed [12,13]. Najafi *et al.,* [13] studied hydrofoil-assisted catamarans using various kinds of foil on catamaran ship models. They discovered that foils with an asymmetrical form were more practical to utilize than the others. By installing modified 6-digit Naca airfoils on passenger ships, Firdhaus and Suastika, and Suastika *et al.,* were able to reduce the amount of ship drag by up to 32% [12,14]. Kazemi *et al.,* carried out studies on an asymmetric hull catamaran ship. They found that the installation of an Eppler 385 hydrofoil resulted in a drag reduction that was as high as fifty per cent less than before [15].

The manner in which a hysucat or hysuwac performs hydrodynamically is affected by both the kind of foil used and where on the catamaran the hydrofoils are installed. Furthermore, the vessel's hydrodynamic performance is affected by the lift created by the foils in relation to the vessel's displacement. Retrofitting a foil system onto an existing catamaran, as discussed in this article, requires careful consideration of each situation and constructing a well-thought-out foil system layout. The research on hydrofoil-supported catamarans has not sufficiently explored these subjects in the available literature. With many towing tank experiments and numerical simulations already available in the literature [16-19], the Delft-372 catamaran model will be used in this study, making verifying and validating calculations from the simulation results straightforwardly. The Delft-372 catamaran will have a high Reynolds number 4-digit NACA 4412 airfoils installed on its hull. This airfoil is often used for Wing in Ground (WIG) vehicles and aerodynamically assisted boats [20,21]. Computational fluid dynamics (CFD) simulations were used to examine how the foil system affected the overall resistance of the vessel and its components, including heave, pitch, and wetted surface area.

## 2. Methodology

### *2.1 Free-Surface Solver*

The boundary element technique is used in potential flow programs to investigate the generation of free surface waves [22,23]. The Rankine source technique is used in potential flow algorithms to analyse ship hull-wave interactions and simulate wave resistance [24]. Viscous flow programs may simulate challenges related to free surface phenomena, such as wave-making resistance. These algorithms use two primary approaches for calculating free surface phenomena: the interface-tracking methodology, such as a moving mesh [25], and the interface-capturing method, known as Volume of Fluid (VoF) [26]. In order to model the planning of vessel performance, the numerical simulations will assess different velocities, angles of attack, and trim angles.

The ISIS-CFD flow solver employs the equations of incompressible unsteady Reynolds-averaged Navier Stokes to solve fluid flow problems. The solver spatially discretizes transport equations using the finite volume approach. The face-based method discretizes unstructured meshes, which may be two-dimensional, three-dimensional, or rotationally symmetric. These meshes consist of non-overlapping control volumes bounded by various constitutive features. Eq. (1) to Eq. (3) govern the conservation of mass, momentum, and volume fraction for incompressible multi-phase viscous fluid flow under isothermal circumstances.

$$\frac{\partial}{\partial t}\int_v \rho\, dV + \int_S \rho(\mathbf{U}-\mathbf{U}_d).\mathbf{n}\, dS = 0 \tag{1}$$

$$\frac{\partial}{\partial t}\int_v \rho\, U_i dV + \int_S \rho U_i(\mathbf{U}-\mathbf{U_d}).\boldsymbol{n}\, dS = \int_S (\tau_{ij}I_j - pI_i).\mathbf{n}\, dS + \int_S \rho g_i\, dV \tag{2}$$

$$\frac{\partial}{\partial t}\int_v c_i\, dV + \int_S c_i(\mathbf{U}-\mathbf{U}_d).\mathbf{n}\, dS = 0 \tag{3}$$

A closed surface $S$, travelling at $\mathbf{U}_d$ With an outward-pointing unit normal vector $n$, defines the boundary of the control volume $V$. Fields of velocity ($\mathbf{U}$) and pressure ($\rho$) respectively. The vector $I_j$ It has no components other than the $j$ component, which is 1. $I_j$ Is the tensor of the viscous stress and $g_i$ It is the gravity vector. The presence or absence of fluid $i$ may be deduced from the value of $c_i$, which is the $i$ -th volume fraction.

F. R. Menter's SST (shear-stress transfer) model evolved from two-equation models and has various advantages [27-30]. The model blends coefficients zonally and limits eddy viscosity increase in fast-strained flows. Zonal modelling uses Wilcox's model at solid walls and the conventional model at boundary layer edges and free-shear layers. By restricting turbulent shear stress to a constant multiple of turbulent kinetic energy within boundary layers (a realizability limitation), shear stress transport modelling affects eddy viscosity. This adjustment improves flow prediction with large pressure gradients and separation. The transport equations for the SST k-ω model are:

$$\frac{\partial}{\partial_t}(\rho k) + \frac{\partial}{\partial_{x_i}}(\rho k u_i) = \frac{\partial}{\partial_{x_j}}\left(\Gamma_k \frac{\partial_k}{\partial_{x_j}}\right) + G_k - Y_k \tag{4}$$

$$\frac{\partial}{\partial_t}(\rho \omega) + \frac{\partial}{\partial_{x_i}}(\rho \omega u_i) = \frac{\partial}{\partial_{x_j}}\left(\Gamma_\omega \frac{\partial_\omega}{\partial_{x_j}}\right) + G_\omega - Y_\omega + D_\omega \tag{5}$$

In Eq. (4) and Eq. (5), $G_k$ Is the term that produces turbulent kinetic energy as a result of mean velocity gradients while $G_\omega$ It is the term that reflects the generation of $\omega$. The quantities $k$ and $\omega$, which are respectively denoted by $Y_k$ and $Y_\omega$, are shown to diminish as a result of turbulence. Furthermore, $D_\omega$ is the abbreviation for the cross-diffusion term, while $\Gamma_k$ and $\Gamma_\omega$ Are the abbreviations for the effective diffusivities of $k$ and $\omega$, respectively. With this turbulence model [31], it is possible to correctly anticipate both the establishment and the magnitude of flow separation.

### *2.2 Modelling, Meshing and Boundary Condition*

In ship hydrodynamics, potential and viscous flow models are often used to simulate and analyse the flow patterns around ships. These models are validated by comparing their results with experimental and numerical data from previous studies. The Delft-372 Catamaran Hull [32], seen in

Table 1, is characteristic of a high-speed catamaran hull. The hydrofoil system on the catamaran utilizes a NACA 4412 airfoil with a High Reynolds number. This airfoil has explicitly been placed on the hull of the Delft-372 catamaran.

**Table 1**
Principal dimension of the Delft-372 Catamaran Hull [32]

| Dimension | Symbol | Value |
|---|---|---|
| Length between perpendiculars (m) | $L_{pp}$ | 3.00 |
| Beam overall (m) | $B$ | 0.94 |
| Beam demi hull (m) | $b$ | 0.24 |
| Distance between centre of hulls (m) | $H$ | 0.7 |
| Draught (m) | $T$ | 0.15 |
| Displacement (kg) | $\Delta$ | 87.07 |
| Vertical centre of gravity (m) | $V_{CG}$ | 0.34 |
| Longitudinal centre of gravity (m) | $L_{CG}$ | 1.41 |

Figure 1 displays the configuration of the NACA 4412 foil system on the Delft-372 catamaran. The hydrofoil system comprises two foils, one positioned towards the front of the vessel and the other towards the rear. Figure 1a shows the longitudinal location of the foils, whereas Figure 1b indicates their submerged depth. The submerged depth of the foils was calculated using the equation $h/c$ = 0.4, where $h$ represents the submerged depth, and $c$ means the chord length of the hydrofoil [33]. The span $s$ of the foils is equal to the distance between the catamaran's two hulls, which measures 0.7 meters. The chord length of the foils is 10 centimetres, equivalent to 0.10 meters. The aspect ratio (AR) of the foil is 7, where AR is defined as the ratio of the span ($s$) to the chord ($c$). Prior research on the NACA 4412 indicated that the angle of attack at which the highest lift-to-drag ratio is achieved is between 4° and 6° [34,35]. Hence, the foils were adjusted at an angle of attack of 5.25°, measured in a counterclockwise direction from the vessel's course direction, corresponding to the positive x-axis.

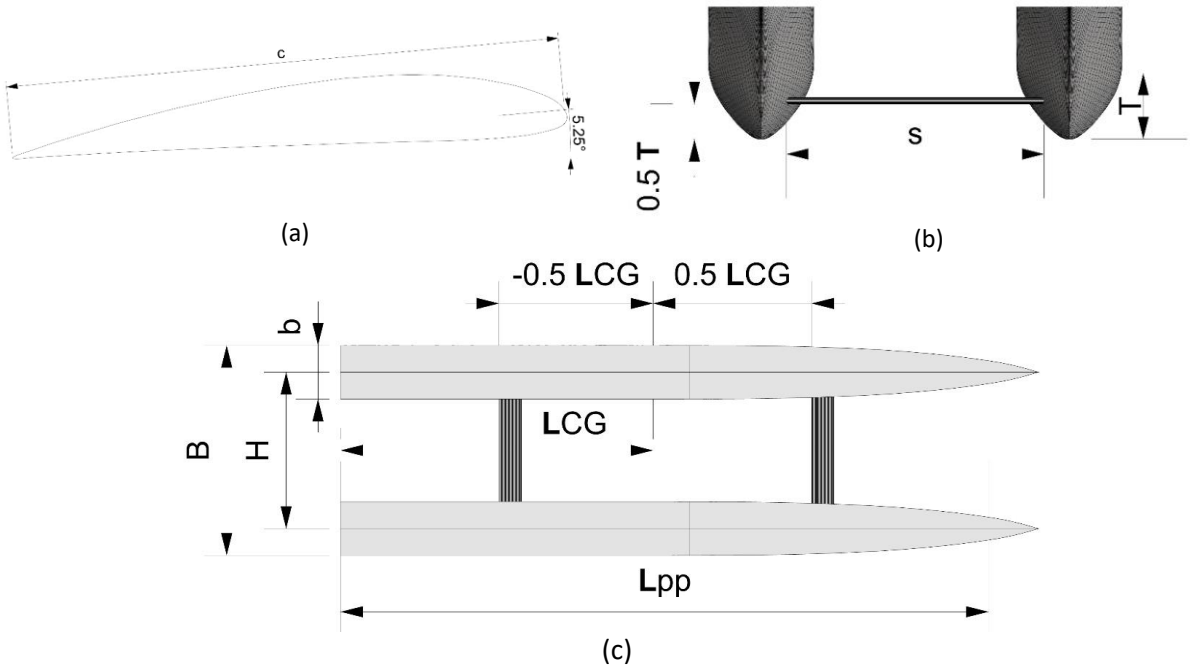


**Fig. 1.** The hydrofoil system used on the Delft-372 catamaran: (a) NACA 4412 foil configuration, (b) foil depth position, and (c) longitudinal position of the hydrofoils

Figure 2 and 3 show a 3-D CAD model of the specified Delft-372 catamaran hull shape and the mesh of the computational domain that incorporates the designated model Delft-372. The geometry was created with the help of the FINE$^{TM}$/Marine modules C-Wizard and HEXPRESS, as well as the NUMECA grid generator [36]. The C-Wizard plugin walks users through configuring mesh and solver parameters. The computational domain is defined by designing a frame around the ship, and the ship's length determines the domain's size, as detailed in Figure 2.

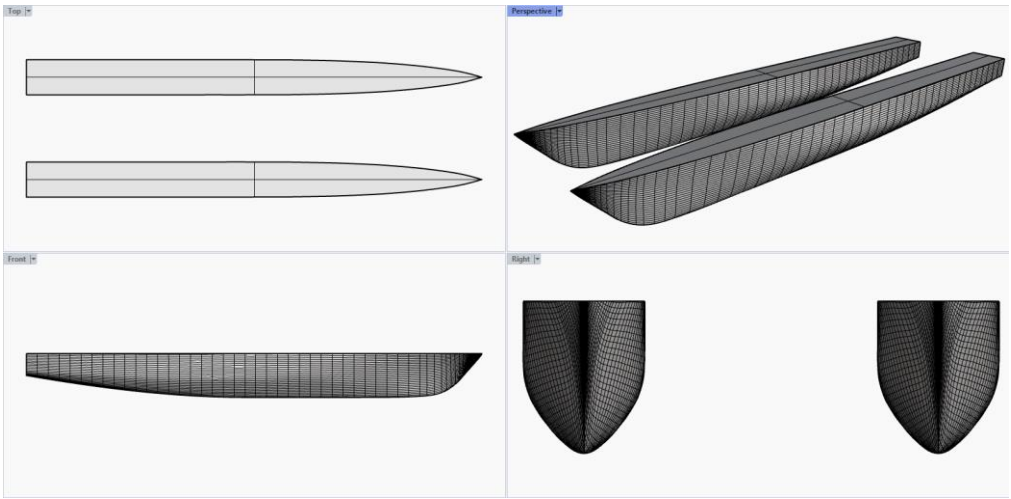

**Fig. 2.** A 3-D CAD model of the designated Delft-372 catamaran hull form

Figure 3 illustrates the computational domain with boundary conditions derived from literature [37]. The intake was located 1L upstream of the model. The outlet was located 3L aft, close to the model's rear. The sidewall was positioned 1.5 times the length (L) away from the waterline. The inlet, exit, and sidewall boundary conditions were all assigned the same free stream far-field velocity. The boundary conditions were set by specifying a fixed pressure, with the bottom and top walls positioned 1.5 times the length of the model below and one times the length above, respectively. The ship's hull used a wall function as the boundary condition to ensure no slip. The simulations also addressed and resolved the heave and pitch motions.

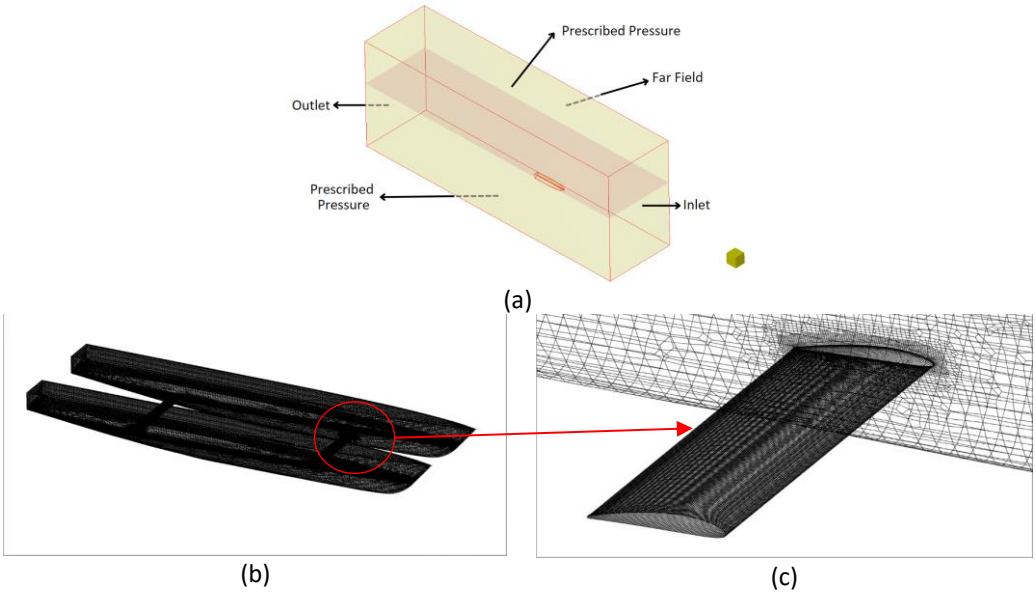


**Fig. 3.** Computational domain and boundary conditions with the simulation model (a) and detail mesh on the surface of the simulation model (b)

The wall distance (Y+) is used within the region where the viscosity impact between the wall and the turbulent zone is significant. Y+ is the dimensionless distance between the first grid node and the wall surface, normalized by the local viscous length scale. The International Towing Tank Conference (ITTC) in 2011 suggests that the Y+ value should be within the range of 30 < Y+ < 100. The calculation is performed using the following formula. The ship's Y+ value, as seen in Figure 4, value within the range of 45 to 75 on average.

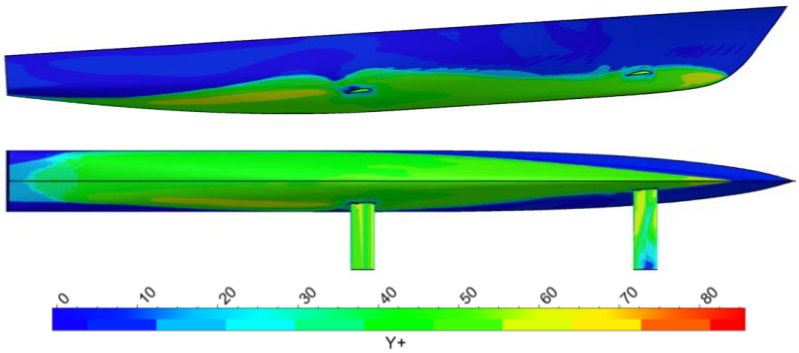


**Fig. 4**. Wall Y+ on hydorofil supported catamaran at Fr = 0.65

*2.3 Grid Independency Study*

The stability of solution should be assessed concerning mesh refinement. A solution is considered mesh-independent when further grid refinement does not significantly alter the results. Relying on a stable and mesh-independent solution is important for result reliability. In order to determine the optimum grid size (number of cells) and to investigate the convergence of the numerical solution to fulfil the grid-independence criterion [38], studies involving grid independence were carried out. The total ship resistance ($R_T$) was calculated by increasing the number of cells in the simulation. Multiple simulation runs are performed, with the number of grids rising by 1.5 to 2 with each run. Each simulation's completion time was measured against the others, and the difference was reported as a percentage.

Ship resistance as a function of simulated cell count approaches a convergence point in Table 2 and Figure 5, with the trend attaining an asymptotic value as the cell count approaches infinity. The optimal number of cells is regarded as 1.91 x $10^6$ cells (run number 5th) with a percent error of 0.63%, significantly less than the 2% suggested in the literature [39].

**Table 2**
The resistance of a ship ($R_T$) is calculated by increasing the number of cells in the simulation

| No | Cells Amount | $R_T$ (N) | Percentage error [%] |
|---|---|---|---|
| 1 | 0.28 x $10^6$ | 13.46 | |
| 2 | 0.56 x $10^6$ | 12.91 | -4.25% |
| 3 | 0.84 x $10^6$ | 12.57 | -2.66% |
| 4 | 1.27 x $10^6$ | 12.32 | -2.05% |
| 5 | 1.91 x $10^6$ | 12.24 | -0.63% |
| 6 | 3.82 x $10^6$ | 12.25 | 0.02% |

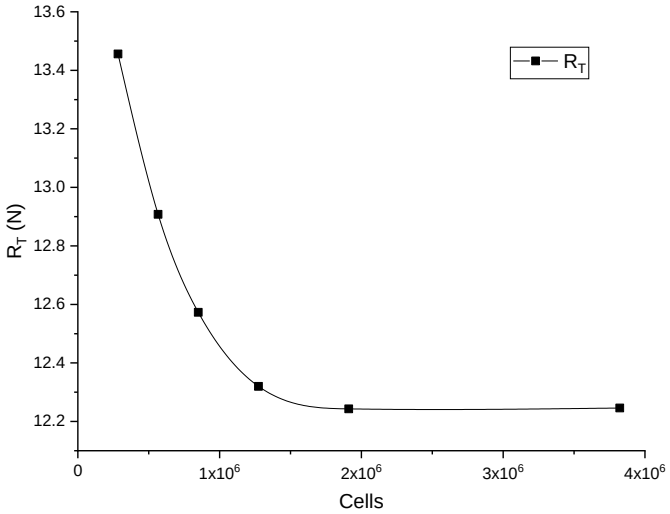


**Fig. 5.** Overall vessel drag function ($R_T$) represents the total number of cells used in the simulation

## 3. Results

### *3.1 Ship Resistance*

This section presents the results of the computational fluid dynamics (CFD) simulation for the overall resistance of the catamaran, both with and without the foil system. The Delft-372 catamaran barehull (BH) and hydrofoil-supported catamaran (HYSUCAT) are simulated at five speeds ranging from Fr 0.3 to 1.4 to determine the ship's total resistance. The simulation results in the value of the total resistance of the ship denoted as $R_T$. In order to validate the results, the CFD simulation findings were compared to experimental data obtained from prior research. This study focused on just one process validation parameter, namely total resistance. Additional factors, such as dynamic trim and sinkage, will be discussed in the subsequent section. Analysis of Computational Fluid Dynamics (CFD) and Experimental Fluid Dynamics (EFD) findings demonstrates significant discrepancies over the whole range of speeds. The resistance prediction is deemed satisfactory, with an average absolute error value not exceeding 5%, which is considered very acceptable for resistance simulations.

Table 3 and Figure 6 demonstrate that the retrofit of the foil system increases total resistance at Fr 0.8 but decreases at Fr > 1. Specifically, the resistance increases to 33.52%, with the most significant increase occurring when the ship travels at the slowest speed, Fr = 0.3, and then reducing with faster speeds up to Fr 0.8, where the resistance increases by 9.95%. In addition, when Fr > 1, the foil system decreases the total resistance by 8.9% at Fr = 1 and 41.83% at the service speed (Fr = 1.4). At moderate velocities, the foil's lift is insufficient to elevate the vessel, increasing its attachment resistance. Foils generate a greater lift force at high speeds, decreasing vessel resistance. The 32.04 per cent decrease in total resistance at service speed is encouraging in light of the foil system's intended to function as an energy-saving device. The observed dynamic trim and sinkage results and the wetted surface area (WSA) of the vessel will be used to analyse the observations mentioned in greater depth in the following section.

**Table 3**
Comparison between EFD and CFD simulation of both barehull and hysucat model for ship resistance

| Fr | Experiment (N) | CFD (N) | | Percentage Difference % | |
|---|---|---|---|---|---|
| | | Barehull | Hysucat | Validation (Barehull v. Experiment) | Hysucat v. Barehull |
| 0.3 | 13.113 | 12.664 | 16.908 | -3.42 | 33.52 |
| 0.45 | 43.243 | 41.664 | 52.686 | -3.65 | 26.45 |
| 0.55 | 59.237 | 56.737 | 68.516 | -4.22 | 20.76 |
| 0.65 | 68.173 | 65.357 | 77.484 | -4.13 | 18.55 |
| 0.8 | 86.198 | 82.869 | 91.115 | -3.86 | 9.95 |
| 1 | - | 116.726 | 106.305 | - | -8.93 |
| 1.2 | - | 164.199 | 120.544 | - | -26.59 |
| 1.4 | - | 234.332 | 136.314 | - | -41.83 |

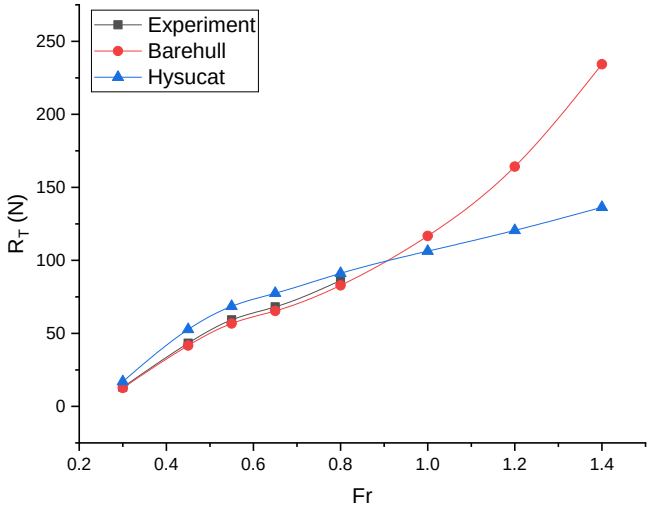


**Fig. 6.** Overall ship resistance ($R_T$) as a function of ship Froude number (Fr)

Figure 7(a)-(d) demonstrate that the wave patterns are composed of transverse waves that travel in the same direction as the vessel's path and divergent waves that travel at an angle to the vessel's course. With increased speed, the wave pattern becomes more characterized by diverging waves. The rise in overall resistance at low velocities resulting from implementing the foil system is partially attributed to the augmentation of wave-making resistance. These data align with the conventional analytical expectations outlined by Suastika *et al.,* [14]

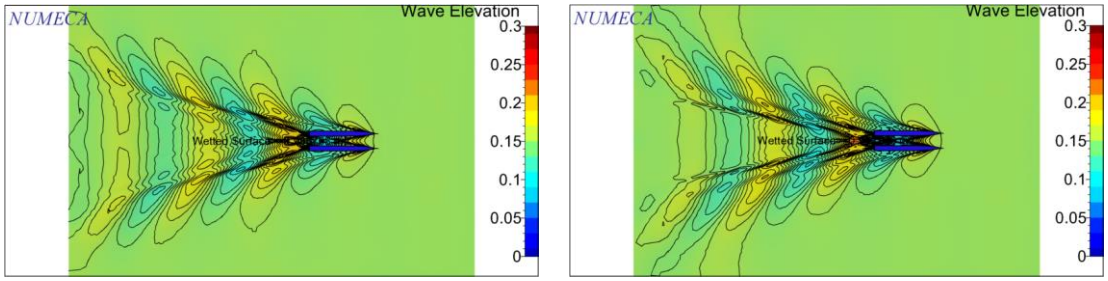


(a) (b)

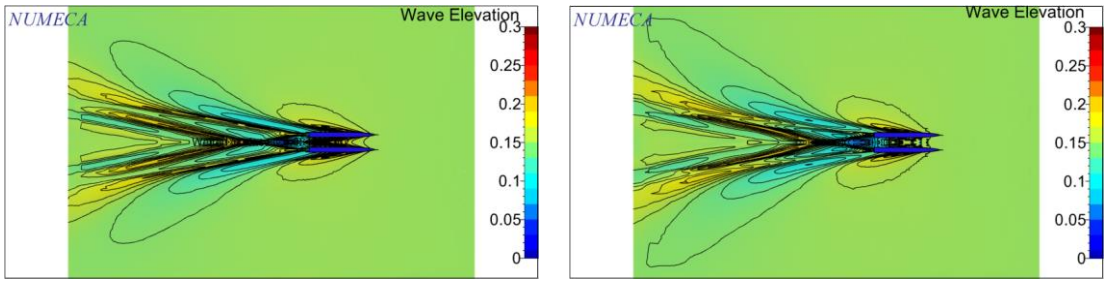


(c) (d)

**Fig. 7.** W The wave patterns for the catamaran are observed under two distinct speed situations, namely, Fr = 0.5 and Fr = 1.4. These conditions are examined for barehull configurations (a and c) and the hysucat (b and d)

Figure 8 and 9 illustrate the fluid's viscous stress vectors acting on the wall. Specifically, Figure 9 provides a more detailed comparison between the base model (8a) and hysucat (8b) at Fr 0.65. The active vector quantity is indicated by an arrow at a specific mesh node on the hull. Figure 8 also incorporates the dynamic vector quantity. The vector magnitude of viscous stress is shown using a colour gradient, spanning from blue to red. Blue represents a value of 0, while red represents a value of 70. Figure 8(a) illustrates a more pronounced shade of light green around the bow and the whole WSA surface. In contrast, Figure 8(b) shows a reduced intensity of blue colour on the hull and a prominent red colour in the hydrofoil region.

Figure 8 indicates that the hydrofoil-supported catamaran has 31.0% and 25.4% more viscous stress than the basic model catamaran for lower Froude numbers (0.3, 0.45). At Froude numbers of 1 and higher, the basic model catamaran reverses, causing greater viscous stress than the hydrofoil-supported catamaran. The hydrofoil-supported catamaran's viscous stress decreases as percentage differences decrease. These statistics imply that Froude number affects viscous stress differently in the two catamaran designs. At lower Froude numbers, the hydrofoil-supported catamaran has more viscous stress than the normal model. At high speeds (Fr > 0.8), the hydrofoil lifts the hull, reducing the wetted surface area and stress.

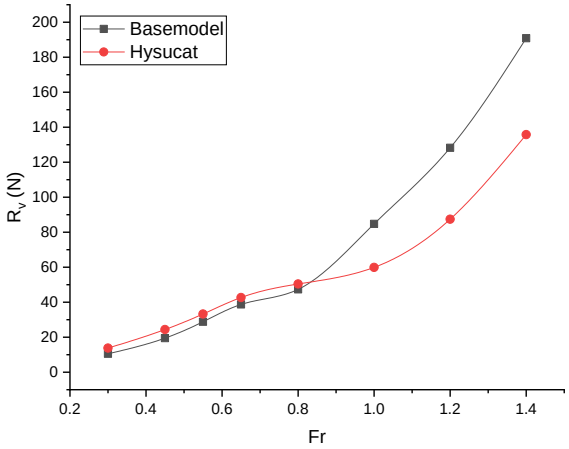


**Fig. 8.** Overall ship viscous stress ($R_v$) as a function of ship Froude number (Fr)

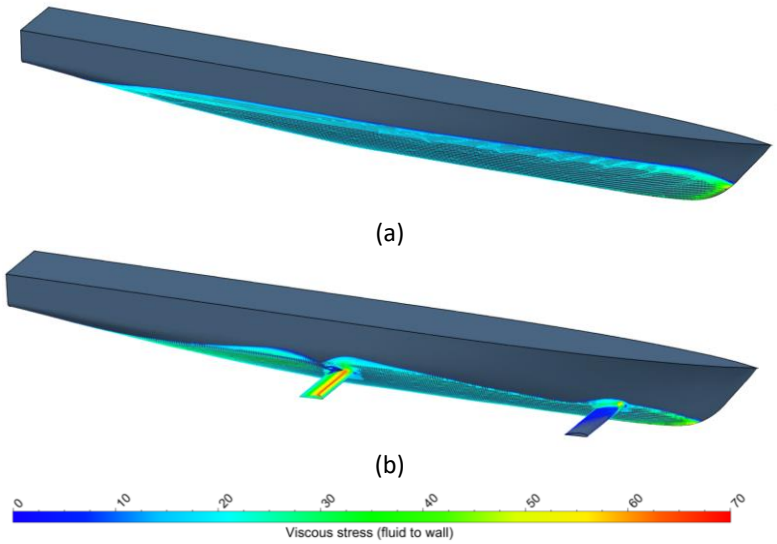


**Fig. 9.** Visual comparison of viscous stress between base model catamaran (a) and hysucat (b) at Fr = 0.65

### *3.2 Pitch and Heave*

The generated resistance is directly proportional to the pressure exerted by the hull, which influences the adjustment of the vessel's trim. Figure 10 illustrates the comparison of the trim at various Froude values. A negative running pitch angle indicates a trim by stern. The pitch angles vary from 0.099° and 3.456°. The hysucat model achieved a maximum pitch angle of -3.450° at Fr 0.65, whereas the barehull model reached a maximum pitch angle of -1.845° at the same Fr. Applying hydrofoil to the catamaran hull results in a reduction in the trim value compared to a catamaran without hydrofoil, especially during the planning phase at Fr < 1, with a drop of up to 26%. The general configuration of the Delft 372-Catamaran Barehull and Hysucat has a similar trend, with the exception of a notable occurrence when the pitch of the Hysucat model experiences a significant and sudden rise at specific velocities. Once the foil forces surpass the hull suction, the pitch angle experiences a rapid rise, leading to an even quicker reduction in suction forces. A type of instability called pitch-up instability occurs when the foil located at the front of the vessel loses lift near the free surface. This instability is eventually suppressed, and the ship reaches a new stable position where the front foil is very close to the free surface, and the hull is planning at a high pitch angle. It is essential to observe that while the foil is in the air, the trim angle lowers as the speed rises.

The vertical oscillations a high-speed catamaran encounters are often known as the heave motion. The ship's capacity to glide over the water's surface generates this motion. Figure 11 compares the heave of the Delft-372 catamaran at various speeds, specifically between the Barehull and Hysucat models. The heave is used as a measure of the dynamic sinkage. At a Fr (Froude number) of 0.3, the displacement phase of the Barehull exhibits a heave value of 0.182 meters, representing a 0.8% increase compared to the hysucat model. However, for a planning phase with Fr larger than 0.8, there is an increase in the heave value by up to 51.5%. On the surface of hysucat, there is a correlation between the increase in heave value and the rise in speed. Excessive vertical movement in a hysucat may decrease hydrodynamic efficiency and a reduction in speed.

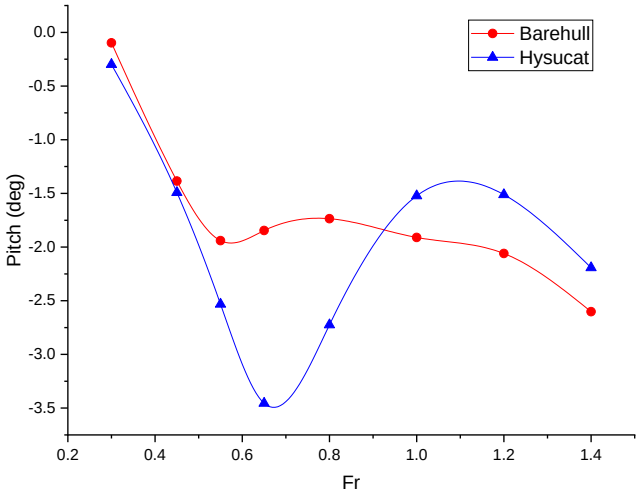


**Fig. 10.** Pitch (deg) as a function of ship speed (Fr)

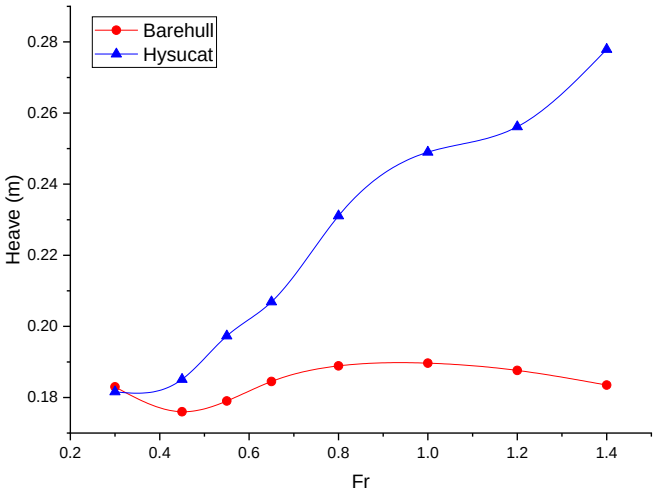


**Fig. 11.** Heave (m) as a function of ship speed (Fr)

### *3.3 Wetted Surface Area*

Table 4 and Figure 12 demonstrate that the foil system retrofit decreases total wetted surface area (WSA). Moving at a moderate pace creates additional lift, and both demihulls get partial support. The alteration in WSA is equivalent to the scenario when foils are not lifted since the primary foil remains completely immersed. The hull experiences strong support at high velocity, causing a decrease in WSA due to the pitch angle and allowing the direct foil to penetrate the surface. In this case, the resistance is anticipated to rise as the pitch angle increases, primarily because of a significant loss of lift on the primary foil.

The WSA of a catamaran decreases as the pitch angle increases until the hull becomes visible above the water surface. This is anticipated to reduce the resistance encountered by the ship. The incorporation of hydrofoils led to a somewhat more intricate connection since there is a decrease in the upward force caused by the angle at which the aircraft is pitched (thus increasing the wing surface area). For instance, when hydrofoil support is almost complete, decreasing the pitch angle would reduce dynamic sinking, hence lowering the WSA. The pitch angle causes the primary foil to rise to the surface, resulting in less lift and promoting ventilation, ultimately reducing ship resistance.

**Table 4**
Percentage comparison of wetted surface area between CFD barehull and hysucat model

| Fr | WSA (m) | | Percentage |
|---|---|---|---|
| | Barehull | Hysucat | Difference % |
| 0.3 | 1.978 | 2.159 | 9.12 |
| 0.45 | 1.962 | 1.984 | 1.15 |
| 0.55 | 1.956 | 1.831 | -6.42 |
| 0.65 | 2.011 | 1.712 | -14.90 |
| 0.8 | 2.017 | 1.558 | -22.73 |
| 1 | 2.104 | 1.470 | -30.14 |
| 1.2 | 2.269 | 1.260 | -44.46 |
| 1.4 | 2.521 | 1.282 | -49.13 |

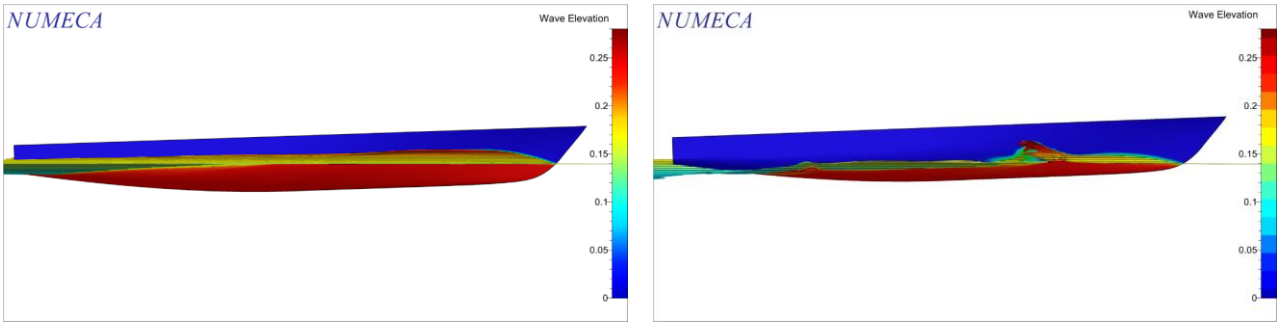


(a) (b)

**Fig. 12.** Visual comparison of wetted surface area between CFD barehull and hysucat model at planning phase (Fr=1.41)

## 4. Conclusions

An existing catamaran was retrofitted with a foil system to improve the vessel's performance. The foil system impacts several factors, such as the wetted surface area, dynamic sinkage and pitch, and the wave pattern produced by the vessel. These factors together influence the overall resistance of the ship. Hydrofoil assistance may decrease the resistance of most catamaran hullforms. The degree of resistance enhancements is heavily contingent upon the hull's shape. Typically, hulls with a significant issue with wave-making resistance may be improved more quickly, but hulls that are already highly efficient tend to have less room for improvement unless the hull is raised much out of the water. An assessment of the transportation efficiency of these vessels, when compared to traditional catamarans, reveals that hydrofoil-assisted catamarans may provide much higher efficiencies than catamarans throughout the planning phase or within the Froude number range Fr > 0.8, up to a maximum of 42%. Hydrofoil-assisted catamarans may be built to have efficiencies that are at least as good as conventional catamarans while operating at lower Froude numbers. The foil system elevated the vessel and decreased its wetted surface area by up to 51%. In addition, it significantly impacts the dynamic sinkage and pitch angle, particularly at high velocities, hence diminishing the wave-making resistance. The foil fraction lift is the primary hydrofoil design characteristic to be considered, with trim improvements of up to 26% in the planning phase. When using high foil lift fractions, it is essential to consider the possibility of directional and pitch-heave instabilities.

Future studies should focus on developing Stability theory for hydrofoil-assisted catamarans in order to have a deeper understanding of the initiation of pitch-heave instabilities.

## Acknowledgement

This research was financed by funding other than the State Revenue and Expenditure Budget (excluding the APBN) of Diponegoro University for the Fiscal Year 2023, under contract number 606-96/UN7.D2/PP/VIII/2023.

## References

[1] Uithof, Kasper, P. Van Oossanen, N. Moerke, P. G. Van Oossanen, and K. S. Zaaijer. "An update on the development of the Hull Vane." In *9th International Conference on High-Performance Marine Vehicles (HIPER), Athens*, pp. 211-221. 2014.
[2] Hoppe, Karl-G. *The hysucat development*. Department of Mechanical Engineering, University of Stellenbosch, 1989.
[3] Barkley, Richard L. "Hydrofoil watercraft." U.S. Patent 3,213,818, issued October 26, 1965.
[4] Homma, N., and J. W. Frouws. "Airfoil Assisted Catamarans: The price of lift is drag." *Ships and Offshore Structures* 2, no. 2 (2007): 157-168. https://doi.org/10.1080/17445300701430416
[5] Hoppe, K. G. W. "The Development of a Hydrofoil-Supported-Rigid-Inflatable Boat." (2001).
[6] Hoppe, K. G. "Optimisation of hydrofoil-supported planing catamarans." *Fast Sea Transportation* (1995).
[7] Hoppe, K. G. "Performance Evaluation of High Speed Surface Craft with Reference to the Hysucat Development." (1991).
[8] Hoppe, K. G. "Recent applications of hydrofoil-supported-catamarans." *Fast Ferry International* 36 (2001).
[9] Manoharan, Raveendran, and Prasanta K. Sahoo. "Drag reduction of NPL round bilge hull forms in HYSUCAT configuration: An analytical study." In *7th Int. Conf. High-Performance Marine Vehicles, Melbourne, Florida, USA*, pp. 235-251. 2010.
[10] Manoharan, Raveendran, and Prasanta K. Sahoo. "Drag reduction of NPL round bilge hull forms in HYSUCAT configuration: An analytical study." In *7th Int. Conf. High-Performance Marine Vehicles, Melbourne, Florida, USA*, pp. 235-251. 2010.
[11] Suastika, Ketut, Regi Y. Dikantoro, Dedi B. Purwanto, Dony Setyawan, and Wing HA Putra. "Analysis of Lift and Drag of Mono-foil Hysucat due to Longitudinal Foil-placement Variation." *International Journal of Marine Engineering Innovation and Research* 2, no. 2 (2018). https://doi.org/10.12962/j25481479.v2i2.3655
[12] Firdhaus, Ahmad, and I. Ketut Suastikab. "Experimental and Numerical Study of Effects of the Application of Hydrofoil on Catamaran Ship Resistance." *Revolution* 4 (2022): 104-110.
[13] Najafi, Amin, Hashem Nowruzi, and Hassan Ghassemi. "Performance prediction of hydrofoil-supported catamarans using experiment and ANNs." *Applied Ocean Research* 75 (2018): 66-84. https://doi.org/10.1016/j.apor.2018.02.017
[14] Suastika, Ketut, Gilbert Ebenezer Nadapdap, Muhammad Hafiz Nurwahyu Aliffrananda, Yuda Apri Hermawan, I. Ketut Aria Pria Utama, and Wasis Dwi Aryawan. "Resistance Analysis of a Hydrofoil Supported Watercraft (Hysuwac): A Case Study." *CFD Letters* 14, no. 1 (2022): 87-98. https://doi.org/10.37934/cfdl.14.1.8798
[15] Kazemi Moghadam, H., Rouzbeh Shafaghat, and A. Hajiabadi. "Foil application to reduce resistance of catamaran under high speeds and different operating conditions." *International Journal of Engineering* 32, no. 1 (2019): 106-111. https://doi.org/10.5829/ije.2019.32.01a.14
[16] Zaghi, Stefano, Riccardo Broglia, and Andrea Di Mascio. "Experimental and numerical investigations on fast catamarans interference effects." *Journal of Hydrodynamics, Ser. B* 22, no. 5 (2010): 528-533. https://doi.org/10.1016/S1001-6058(09)60250-X
[17] Broglia, Riccardo, Stefano Zaghi, and Andrea Di Mascio. "Numerical simulation of interference effects for a high-speed catamaran." *Journal of marine science and technology* 16 (2011): 254-269. https://doi.org/10.1007/s00773-011-0132-3
[18] Bouscasse, Benjamin, Riccardo Broglia, and Frederick Stern. "Experimental investigation of a fast catamaran in head waves." *Ocean engineering* 72 (2013): 318-330. https://doi.org/10.1016/j.oceaneng.2013.07.012
[19] Broglia, R., B. Bouscasse, B. Jacob, A. Olivieri, S. Zaghi, and F. Stern. "Calm water and seakeeping investigation for a fast catamaran." In *Proceedings of the 11th international conference on fast sea transportation (FAST2011), Honolulu*. 2011.
[20] Frère, Ariane, Koen Hillewaert, Philippe Chatelain, and Grégoire Winckelmans. "High Reynolds number airfoil: from wall-resolved to wall-modeled LES." *Flow, Turbulence and Combustion* 101 (2018): 457-476. https://doi.org/10.1007/s10494-018-9972-9
[21] Ockfen, Alex E., and Konstantin I. Matveev. "Aerodynamic characteristics of NACA 4412 airfoil section with flap in extreme ground effect." *International Journal of Naval Architecture and Ocean Engineering* 1, no. 1 (2009): 1-12. https://doi.org/10.3744/JNAOE.2009.1.1.001

[22] Hess, John L., and Apollo Milton Olin Smith. "Calculation of nonlifting potential flow about arbitrary three-dimensional bodies." *Journal of ship research* 8, no. 04 (1964): 22-44. https://doi.org/10.5957/jsr.1964.8.4.22
[23] Insel, Mustafa. "An investigation into the resistance components of high speed displacement catamarans." PhD diss., University of Southampton, 1990.
[24] Jensen, G., H. Soding, and Z. Mi. "Rankine source methods for numerical solutions of the steady wave resistance problem." In *Symposium on Naval Hydrodynamics, 16th*. 1986.
[25] Li, Tingqiu, and Jerzy Matusiak. "Simulation of modern surface ships with a wetted transom in a viscous flow." In *ISOPE International Ocean and Polar Engineering Conference*, pp. ISOPE-I. ISOPE, 2001.
[26] Raessi, Mehdi, Javad Mostaghimi, and Markus Bussmann. "A volume-of-fluid interfacial flow solver with advected normals." *Computers & Fluids* 39, no. 8 (2010): 1401-1410. https://doi.org/10.1016/j.compfluid.2010.04.010
[27] Menter, Florian R. "Performance of popular turbulence model for attached and separated adverse pressure gradient flows." *AIAA journal* 30, no. 8 (1992): 2066-2072. https://doi.org/10.2514/3.11180
[28] Menter, Florian R. "Influence of freestream values on k-omega turbulence model predictions." *AIAA journal* 30, no. 6 (1992): 1657-1659. https://doi.org/10.2514/3.11115
[29] Menter, Florianr. "Zonal two equation kw turbulence models for aerodynamic flows." In *23rd fluid dynamics, plasmadynamics, and lasers conference*, p. 2906. 1993. https://doi.org/10.2514/6.1993-2906
[30] Menter, Florian R. "Two-equation eddy-viscosity turbulence models for engineering applications." *AIAA journal* 32, no. 8 (1994): 1598-1605. https://doi.org/10.2514/3.12149
[31] Bardina, J., P. Huang, T. Coakley, J. Bardina, P. Huang, and T. Coakley. "Turbulence modeling validation." In *28th Fluid dynamics conference*, p. 2121. 1997. https://doi.org/10.2514/6.1997-2121
[32] Van't Veer, A. P. "Experimental results of motions, hydrodynamic coefficients and wave loads on the 372 Catamaran model." (1998).
[33] Abbott, Ira H., and Albert E. Von Doenhoff. *Theory of wing sections: including a summary of airfoil data*. Courier Corporation, 2012.
[34] Effendy, Marwan, and Muchlisin Muchlisin. "Studi Eksperimental dan Simulasi Numerik Karakteristik Aerodinamika Airfoil NACA 4412." *ROTASI* 21, no. 3 (2019): 147-154. https://doi.org/10.14710/rotasi.21.3.147-154
[35] Haque, M. Nazmul, Mohammad Ali, and Ismat Ara. "Experimental investigation on the performance of NACA 4412 aerofoil with curved leading edge planform." *Procedia Engineering* 105 (2015): 232-240. https://doi.org/10.1016/j.proeng.2015.05.099
[36] NUMECA International, "FINE/Marine 7.2 Theory Guide," *NUMECA online documentation platform,* 2018.
[37] Versteeg, Henk Kaarle, and Weeratunge Malalasekera. *An introduction to computational fluid dynamics: the finite volume method*. Pearson education, 2007.
[38] John, D., and J. R. Anderson. "Computational fluid dynamics: the basics with applications." *Mechanical engineering series* (1995): 261-262.
[39] Hughes, G. *An analysis of ship model resistance into viscous and wave components*. NPL, 1965.
[40] Ghassemi, Hassan, and Mahmoud Ghiasi. "A combined method for the hydrodynamic characteristics of planing crafts." *Ocean Engineering* 35, no. 3-4 (2008): 310-322. https://doi.org/10.1016/j.oceaneng.2007.10.010